Supporting Information

Manganese-Based Oxygen Evolution Catalysts Boosting Stable Solar-Driven Water Splitting: MnSe as An Intermetallic Phase

Mao Sun,[1] Rui-Ting Gao,[1] Xianhu Liu,[2] Rui Gao,[1,*] Lei Wang [1,2,*]

[1] *School of Chemistry and Chemical Engineering & Inner Mongolia Engineering and Technology Research Center for Catalytic Conversion and Utilization of Carbon Resource Molecules, Inner Mongolia University, 235 West University Street, Hohhot 010021, China*

E-mail: gaorui@imu.edu.cn; wanglei@imu.edu.cn

[2] *Key Laboratory of Materials Processing and Mold, Ministry of Education, Zhengzhou University, Zhengzhou 450002, China*

EXPERIMENTAL

Electrocatalysts and photoelectrodes preparation

Preparation of MnSe/NF, MnFeSe/NF, MnCoSe/NF, MnNiSe/NF, and MnSe/FF electrodes.

The Ni foam (NF, Innochem. Co. Ltd.) was cleaned by sonication in acetone, ethanol, and water for 30 min each. The MnO_2/NF was synthesized using a hydrothermal method. Briefly, 0.5 mmol of $KMnO_4$ was dissolved in 30 mL deionized water under mechanical stirring. Then, the resulting solution was transferred to a 50 mL Teflon-lined autoclave containing a piece of NF for reaction at 160 ℃ for 12 h. After cooling down to room temperature naturally, the MnO_2/NF was washed with distilled water and dried in air. The MnO_2/NF samples were then immersed in 10 mM $Fe(NO_3)_3$, $Co(NO_3)_2$, and $Ni(NO_3)_2$ aqueous solutions for cation exchange to obtain Fe-MnO_2/NF, Co-MnO_2/NF, and Ni-MnO_2/NF, respectively.

The formation of MnFeSe/NF, MnCoSe/NF, and MnNiSe/FF were fabricated by hydrothermal treatment using NaHSe as Se source.[1] Specially, the 65 mg $NaBH_4$ was added into 3 mL deionized water. Then the 59 mg Se powder was added into the above solution. After stirring for 20 min, the freshly prepared NaHSe solution was added into 20 mL ethanol under N_2 flow. The solution was transferred into 50 mL Teflon-lined autoclave with the Fe-MnO_2/NF, Co-MnO_2/NF, and Ni-MnO_2/NF for reaction at 140 ℃ for 20 h. After cooling down, the samples were collected and washed with water several times, and dried at 60 ℃ for 6 h. For the formation of MnSe/FF, the iron foil (FF, Kunshan Kuangxun Electrical. Co. Ltd.) was used, and the reaction process was following a two-step hydrothermal process without the Fe immersion for cation exchange.

Preparation of $BiVO_4$, Se-MnO_x/$BiVO_4$, Fe-MnO_x/$BiVO_4$, and Se,Fe-MnO_x/$BiVO_4$ photoelectrodes.

The $BiVO_4$ photoanodes were synthesized according to the reported method.[2] First, $Bi(NO_3)_3 \cdot 5H_2O$ (1.9440 g) was added into 100 mL deionized water containing KI (6.6410g) by adding HNO_3 to attain the pH =1.7. Subsequently, the above solution was mixed with 40 mL ethanol containing p-benzoquinone (0.9944g), and vigorously stirred for a few minutes. Secondly, the electrodeposition of BiOI films was conducted in a three-electrode setup with the fluorine-doped tin oxide (FTO) as the working electrode, the saturated Ag/AgCl as the reference electrode, and the Pt foil as the auxiliary electrode. Cathodic deposition was performed potentiostatically at -0.1 V vs. Ag/AgCl for 5 min at room temperature. Afterward, 0.2 M vanadyl acetylacetonate ($VO(acac)_2$) was prepared, and the freshly prepared solution was placed on the BiOI electrode. The sample was heated to convert BiOI to $BiVO_4$ in a muffle furnace (KSL-1100X-S,

Kejing, China) at 450 °C for 2 h. The annealed sample was then immersed in 1 M NaOH solution for 30 min with stirring to remove the excess V_2O_5. Finally, The $BiVO_4$ was rinsed with deionized water and dried in air.

The $MnO_x/BiVO_4$ was synthesized using a hydrothermal method, which was same to the MnO_x/NF. The NF was used to replace $BiVO_4$. Then, the $MnO_x/BiVO_4$ was immersed in 10 mM $Fe(NO_3)_3$ aqueous solution for 10 min. After that, the sample was washed with deionized water and dried. Dur to the corrosion of $BiVO_4$ in the hydrothermal reaction containing NaHSe, the thermal annealing treatment was replaced in a Se powder as a dopant. The above sample was further annealed in a tube furnace (OTF-1200X-S60, Kejing, China) at 350 ˚C for 30 min in Ar with Se powder as the dopant to form Se,Fe-$MnO_x/BiVO_4$. The Se-$MnO_x/BiVO_4$ and Fe-$MnO_x/BiVO_4$ were prepared with the same approach without Fe immersion or Se dopant.

For comparison, the FeOOH/$BiVO_4$ and FeOOH/$MnO_x/BiVO_4$ were fabricated through a facile solution impregnation method at room temperature. The as-prepared $BiVO_4$ and $MnO_x/BiVO_4$ were immersed in 10 mM $Fe(NO_3)_3$ aqueous solution for 10 min, respectively. Meanwhile, the $MnO_x/BiVO_4$, FeOOH/$BiVO_4$, and FeOOH/$MnO_x/BiVO_4$ were also annealed in Ar at 350 ˚C for 30 min without Se dopant. The Se,Fe-MnO_x electrocatalyst were prepared on NF with the same approach, by replacing $BiVO_4$ with NF.

Characterization

Scanning electron microscopy (SEM) and transmission electron microscopy (TEM) images were taken using Hitachi S-4800 system and FEI Tecnai TF20 microscope. XRD characterization was performed using a Philips X'Pert Pro X-ray diffractometer with a monochromatized Cu Kα radiation source and a wavelength of 0.1542 nm. X-ray photoelectron spectroscopic (XPS) analysis was conducted on an ESCALAB 250Xi spectrometer.

Electrochemical (EC) and Photoelectrochemical (PEC) measurements

The EC measurements, linear sweep voltammetry (LSV) was tested using a CHI 760E electrochemical workstation in 1 M KOH solution from 0 to 0.8 V (vs. Ag/AgCl) at a scan rate of 5 mV s^{-1}. The electrochemical impedance spectroscopy (EIS) was performed over a frequency range from 0.1 Hz to 100

KHz. The electrochemically active surface areas (ECSA) were conducted by cyclic voltammograms (CVs) at different scan rates. Long-term stability was performed by chronopotentiometric measurement at 20 mA cm^{-2} for 20 h. The produced gases were collected by a gas chromatograph (Shimadzu, GC-2014C) every 30 min for 4 h.

For the PEC performance, the measurements were performed under simulated AM 1.5G illumination (100 mW/cm^2, XES-40S3-TT, AAA Class Solar Simulator, Japan) using a CHI 760E electrochemical workstation. 1 M potassium borate aqueous solution (KBi, pH=9.5) was as the electrolyte. The photocurrent vs. voltage (J-V) characteristics were performed by scanning the potential from –0.6 to 0.6 V (vs. Ag/AgCl) with a rate of 10 mV s^{-1}. Long-term stability was performed by at 0.8 V_{RHE} for 20 h. All the potentials were converted to reversible hydrogen electrode (RHE) using the following equation: E_{RHE}= $E_{Ag/AgCl}$+0.197 V+0.059×pH.

DFT Calculation

Methods: All spin polarization calculations were performed using the Vienna Ab Initio simulation package (VASP).[3] The electron-ion interaction was described with the projector augmented wave (PAW) method.[4] The electron exchange and correlation energies were treated within the generalized gradient approximation in the Perdew-Burke-Ernzerhof formalism (GGA-PBE).[5] The energy cutoff of plane wave basis was set to 450 eV, electron smearing width of σ = 0.2 eV was employed according to the Methfessel-Paxton technique, and the MP k-point sampling was utilized. In the calculations, the 3×3×1 k-point sampling was done for all six models. According to the previous studies,[6] the influence of electronic correlations within the GGA+U method was considered for MnOOH, and Se,Fe-MnOOH (Ueff = 3.0 and 4.3 eV for Mn and Fe, respectively), as well as MnO_2 and Se,Fe-MnO_2 (Ueff = 1.6 and 4.0 eV for Mn and Fe, respectively).

As following four elementary steps from (1) to (4) (* in sign of the adsorption site), the whole catalytic cycle of the OER mechanisms were composed, and the changes of Gibbs free energy (Δ*G*) of all these steps were calculated.

$$OH^- + * \rightarrow OH^* + e^- \quad (1)$$

$$OH^* + OH^- \rightarrow O^* + H_2O_{(g)} + e^- \quad (2)$$

$$O^* + OH^- \rightarrow OOH^* + e^- \quad (3)$$

$OOH^* + OH^- \rightarrow O_{2(g)} + H_2O_{(g)} + * + e^-$ (4)

For the overall reaction, the free energy of one OH^- was calculated by $G_{OH^-} = G_{H2O(l)} - G_{H^+}$, in which $G_{H^+} = 1/2G_{H2}$. The free energy of H_2O and H_2 molecule was calculated according to the equation of $G = E + ZPE + TS$, where E is the energy of H_2O or H_2 molecule obtained from DFT calculations; ZPE and S are their zero point energy correction and entropy, respectively, while T is 298K. The entropy of H_2O and H_2 molecule was taken from the standard thermodynamic table, and their ZPE correction is 0.56 and 0.27 eV, respectively, which is from the frequency analysis of DFT calculations.

Models: The calculated lattice constant of MnSe cell is a = b = c = 5.374 Å, and α = β = γ = 90.0°, the calculated lattice constant of MnO_2 cell is a = 2.850 Å, b = 2.849 Å, c = 9.875 Å, α = 89.75°, β = 90.0° and γ = 60.0°, and the calculated lattice constant of MnOOH cell is a = b = 3.137 Å, c = 8.952 Å, α = β = 90.0° and γ = 124.30°. In this work, the unit cell p(2×2) is used for MnSe(100), and Fe-MnSe(100), while the unit cell p(4×4) is used for MnOOH, Se,Fe-MnOOH, MnO_2 and Se,Fe-MnO_2. In total, MnSe(100) has 32 Mn and 32 Se atoms, in which 8 Mn and 8 Se are fixed; Fe-MnSe(100) has 1 Fe, 32 Mn and 31 Se atoms, in which 8 Mn and 8 Se are fixed; MnOOH has 48 Mn, 96 O and 48 H atoms, in which 16 Mn, 32 O and 16 H atoms are fixed; Se,Fe-MnOOH has 1 Fe, 1 Se, 46 Mn, 96 O and 48 H atoms, in which 16 Mn, 32 O and 16 H atoms are fixed; MnO_2 has 48 Mn and 96 O atoms, in which 16 Mn and 32 O atoms are fixed; Se,Fe-MnO_2 has 1 Fe, 1 Se, 46 Mn and 96 O atoms, in which 16 Mn and 32 O atoms are fixed.

References

1. C. Tang, N. Cheng, Z. Pu, W. Xing and X. Sun, *Angew. Chem. Int. Ed.* 2015, **54**, 9351-9355.

2. T. W. Kim and K.-S. Choi, *Science* 2014, **343**, 990-994.

3. a) G. Kresse and J. Furthmuller, *Comp. Mater. Sci.* 1996, **6**, 15-50; b) P. E. Blochl, *Phys. Rev. B: Condens. Matter. Mater. Phys.* 1994, **50**, 17953-17979.

4. a) G. Kresse and J. Furthmuller, *Phys. Rev. B: Condens. Matter. Mater. Phys.* 1996, **54**, 11169-11186; b) G. Kresse and D. Joubert, *Phys. Rev. B* 1999, **59**, 1758-1775.

5. J. P. Perdew, K. Burke and M. Ernzerhof, *Phys. Rev. Lett.* 1996, **77**, 3865-3868.

6. a) Z. Yang, X. Wang and Y. Huang, *Curr. Appl. Phys.* 2015, **15**, 1556-1561; b) S.-M. Xu, H. Yan and M. Wei, *J. Phys. Chem. C* 2017, **121**, 2683-2695.

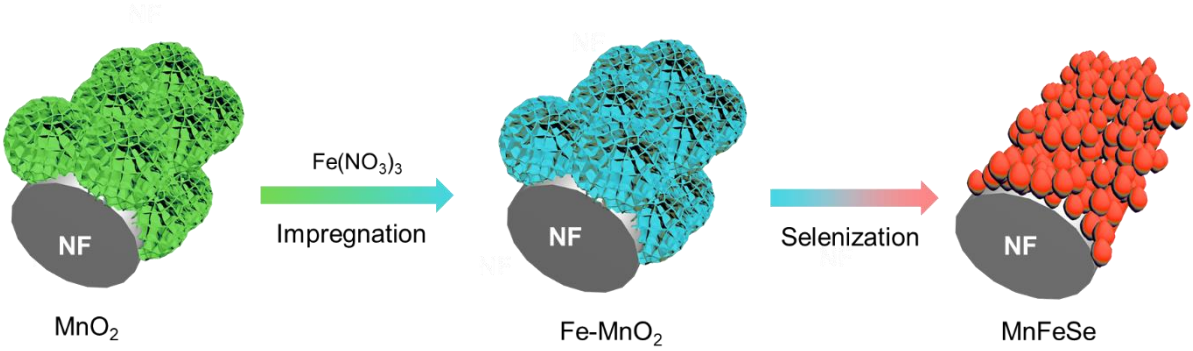

Scheme S1. Schematic illustration for the preparation of MnFeSe on nickel foam.

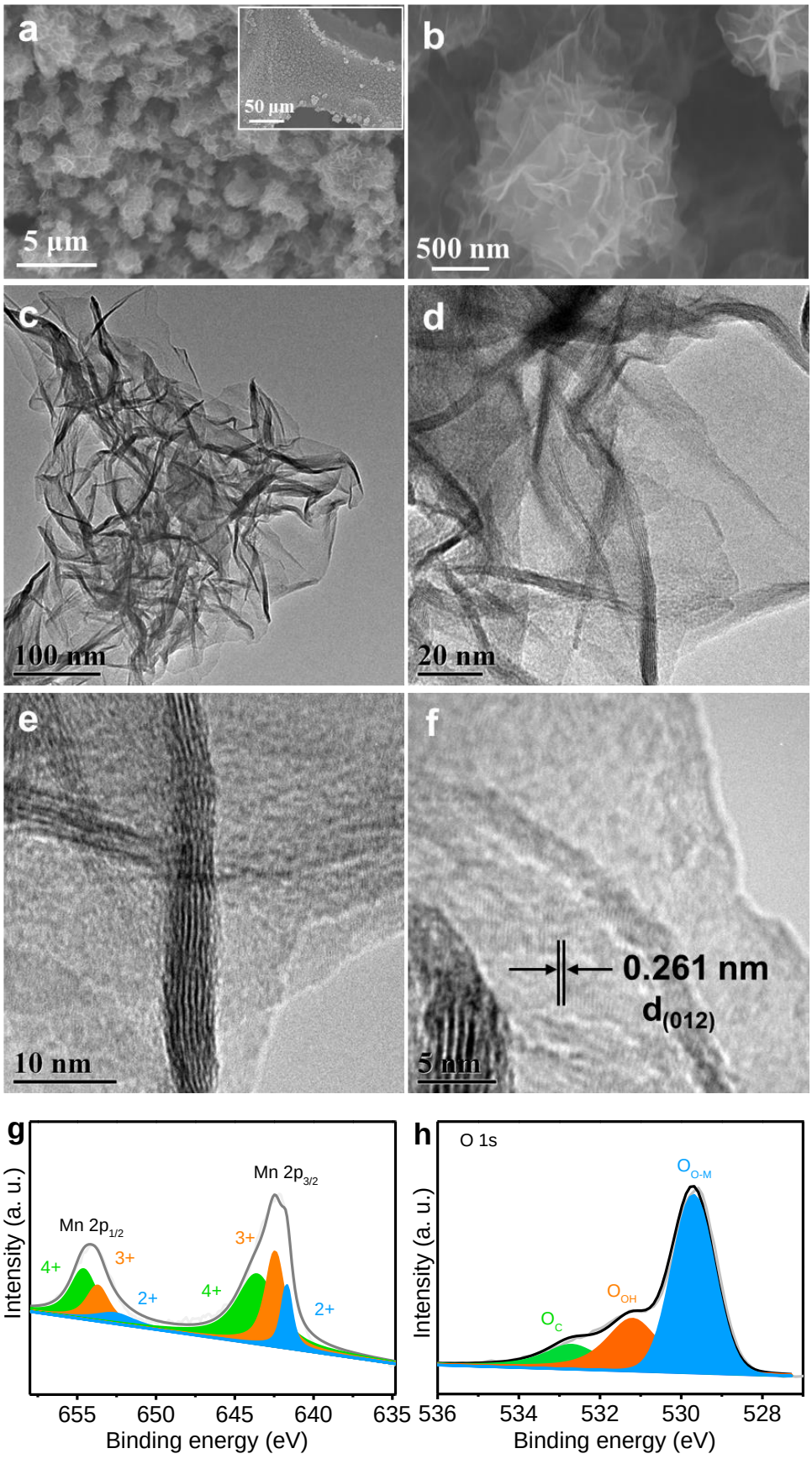

Figure S1. (a,b) SEM, (c-f) TEM images, (g) Mn 2p, and (h) O 1s XPS spectra of MnO_2.

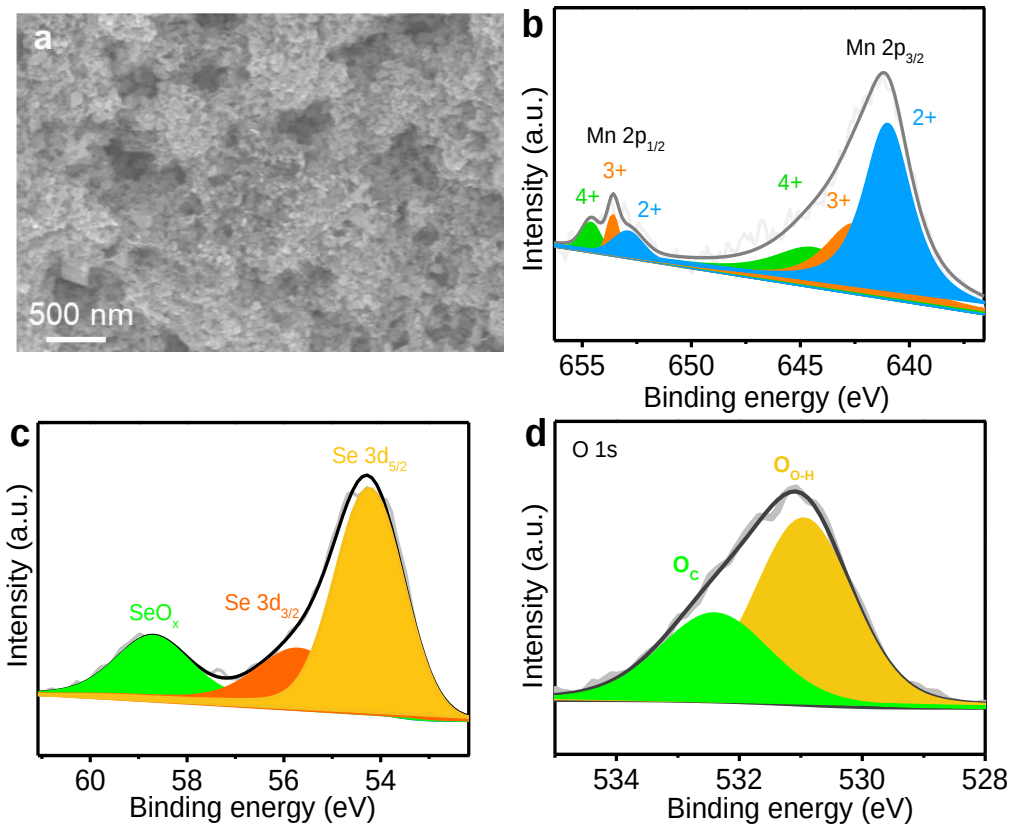

Figure S2. (a) SEM image, (b) Mn 2p, (c) Se 3d, and (d) O 1s XPS spectra of MnSe.

The surface oxidation was confirmed from O 1s XPS spectra (**Figure S2d**), in which two deconvoluted peaks at 531.3 eV and 533.8 eV can be ascribed to surface hydroxylation and water adsorbed onto the surface, respectively.

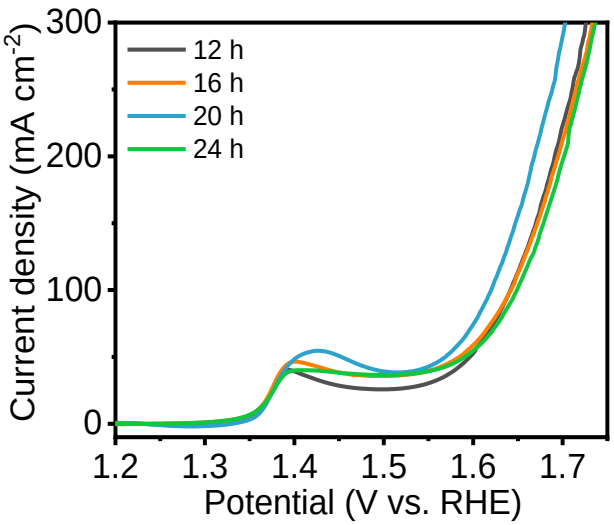

Figure S3. LSV curves for OER of MnSe at 140 °C with different hydrothermal times in 1 M KOH. The optimal reaction condition for OER was at 140 °C for 20 h.

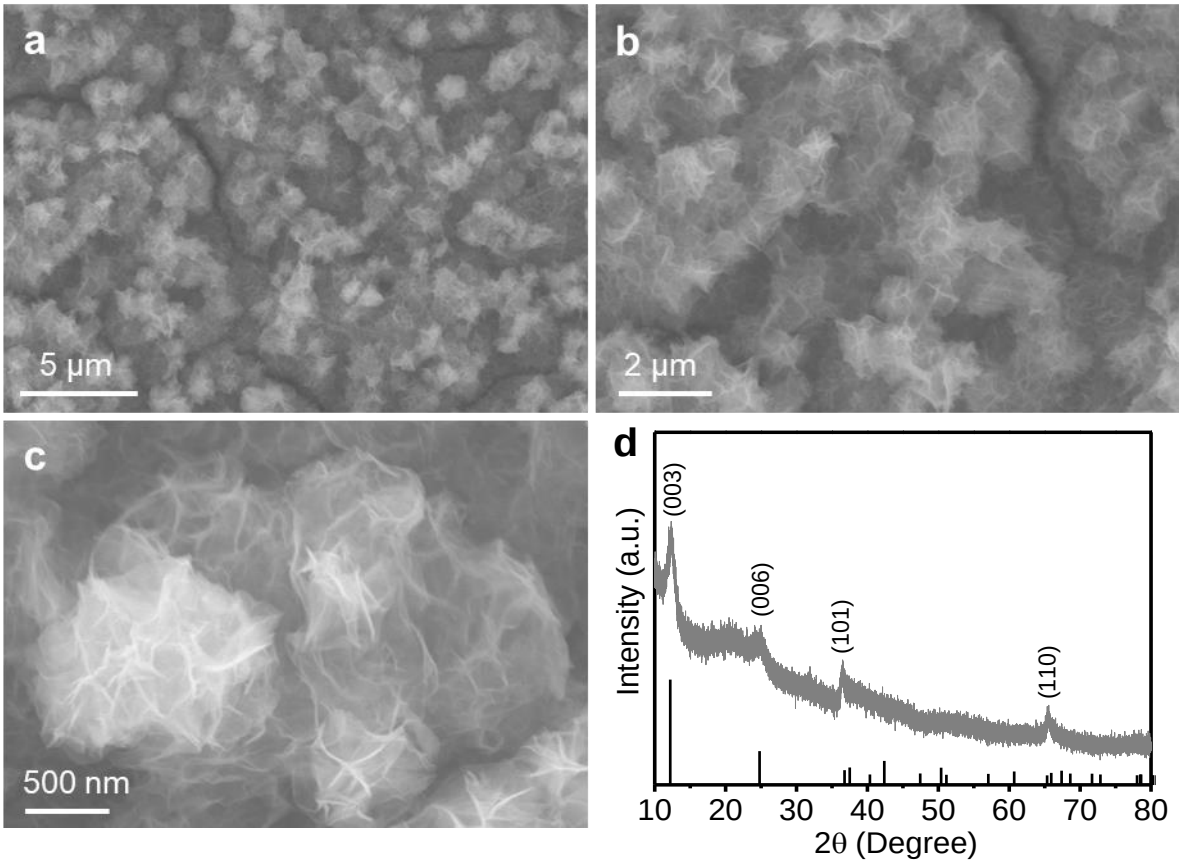

Figure S4. (a-c) SEM images and (d) XRD pattern of Fe-MnO_2. The MnO_2 was immersed into $Fe(NO_3)_3$ for cation exchange.

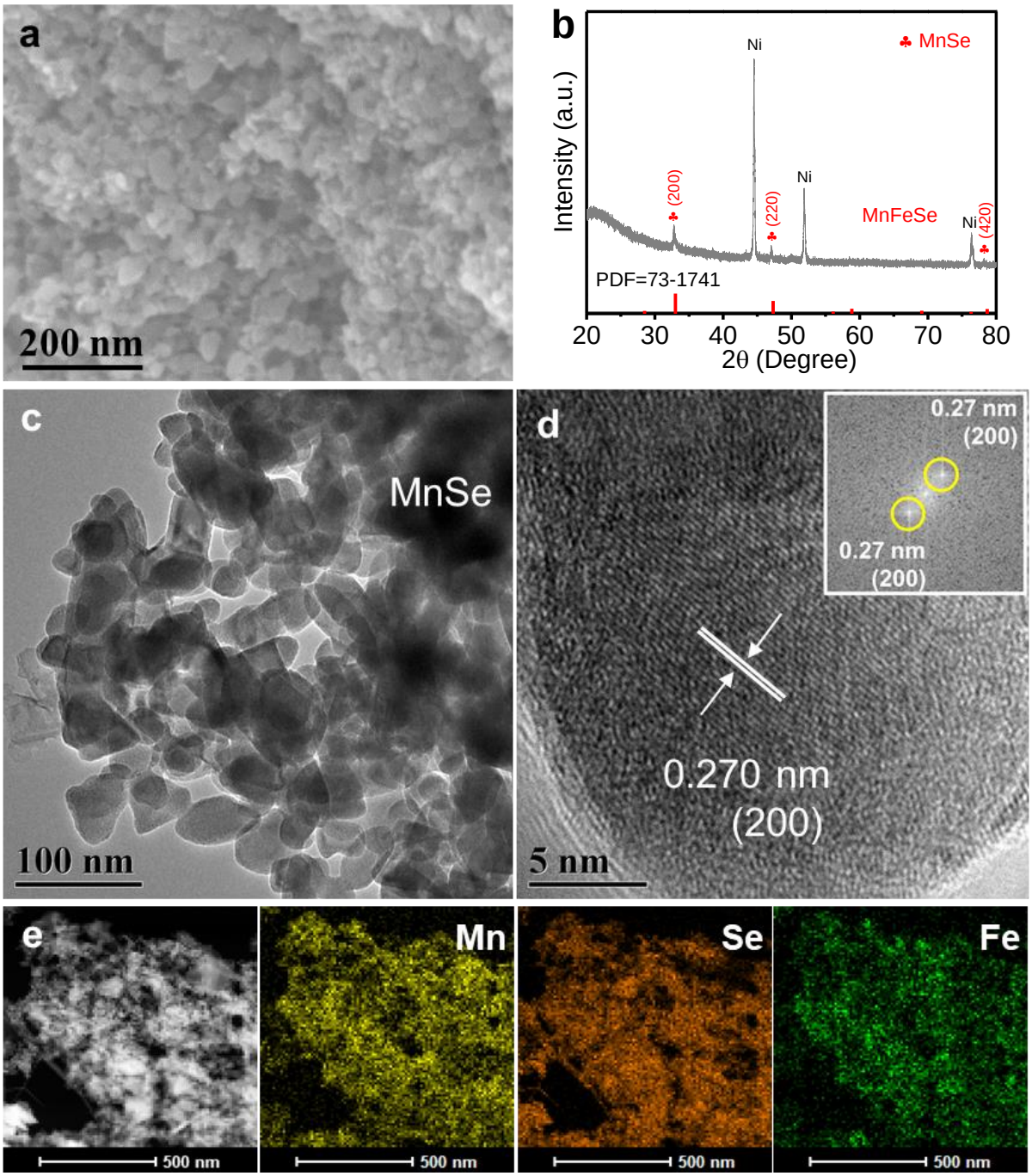

Figure S5. (a) SEM image, (b) XRD pattern, (c) TEM image, (d) HRTEM image, and (e) TEM-EDS elemental mapping of MnFeSe/NF. Inset of d shows the FFT pattern.

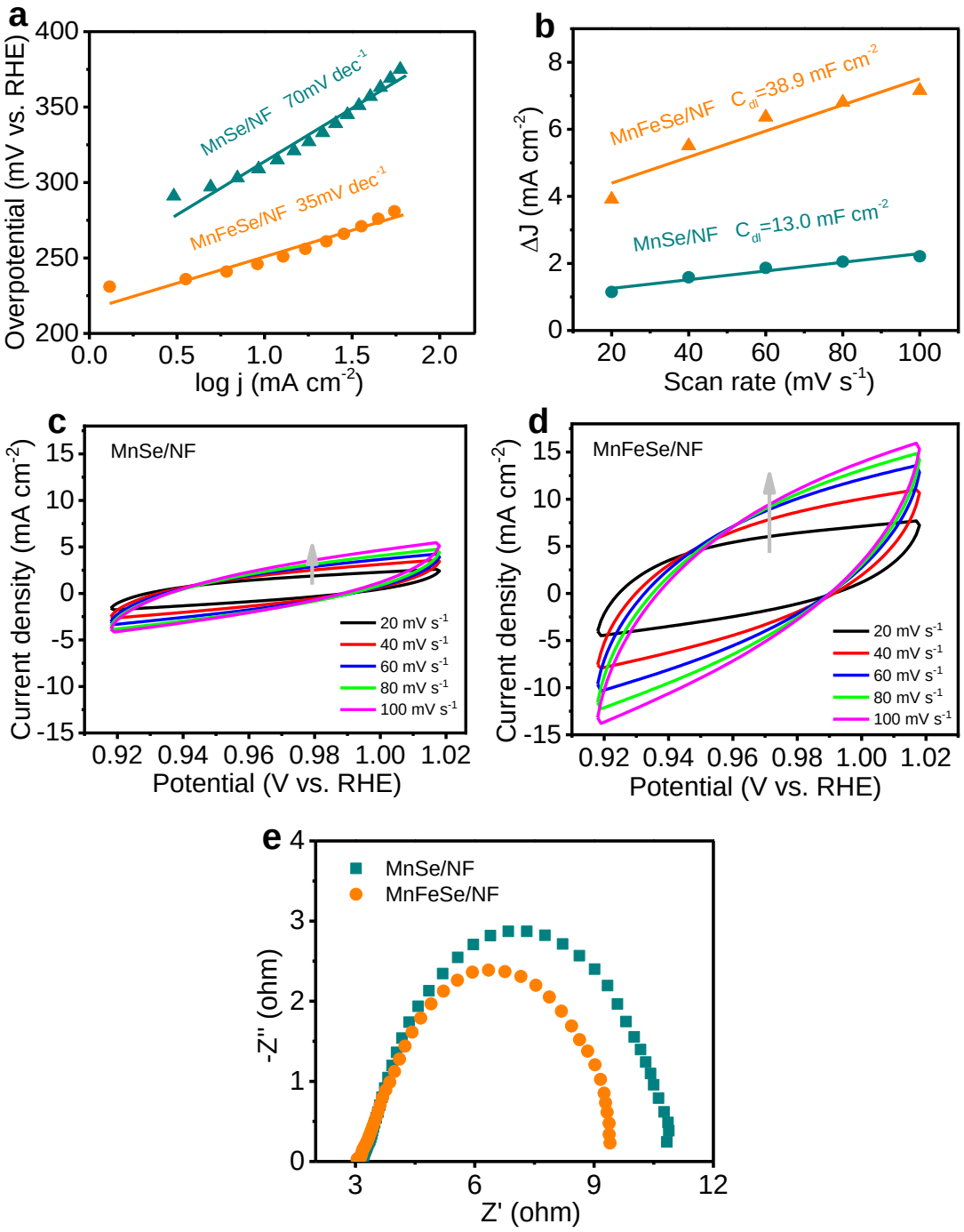

Figure S6. (a) Tafel plots MnSe/NF and MnFeSe/NF; (b) liner fitting of the C_{dl} for the catalysts versus scan rate for the estimation of the ECSA; (c,d) CV curves of MnSe/NF (c) and MnFeSe/NF (d) for OER at different scan rates in 1 M KOH; (e) EIS spectra of MnSe/NF and MnFeSe/NF in 1 M KOH.

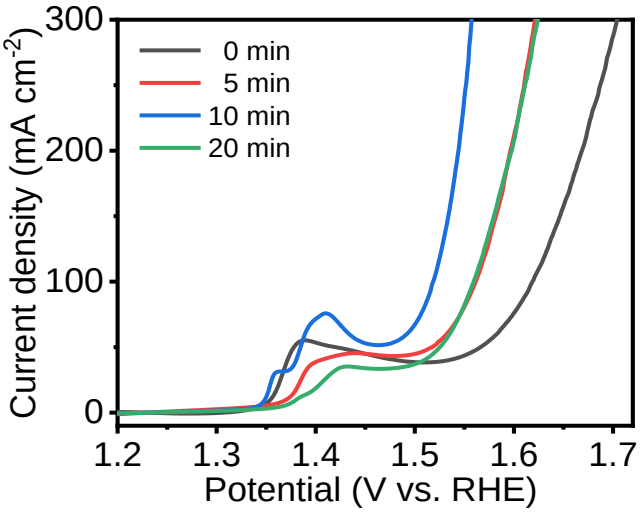

Figure S7. LSV curves for OER of MnFeSe/NF in 1 M KOH. The MnO_2 was immersed into $Fe(NO_3)_3$ for various times.

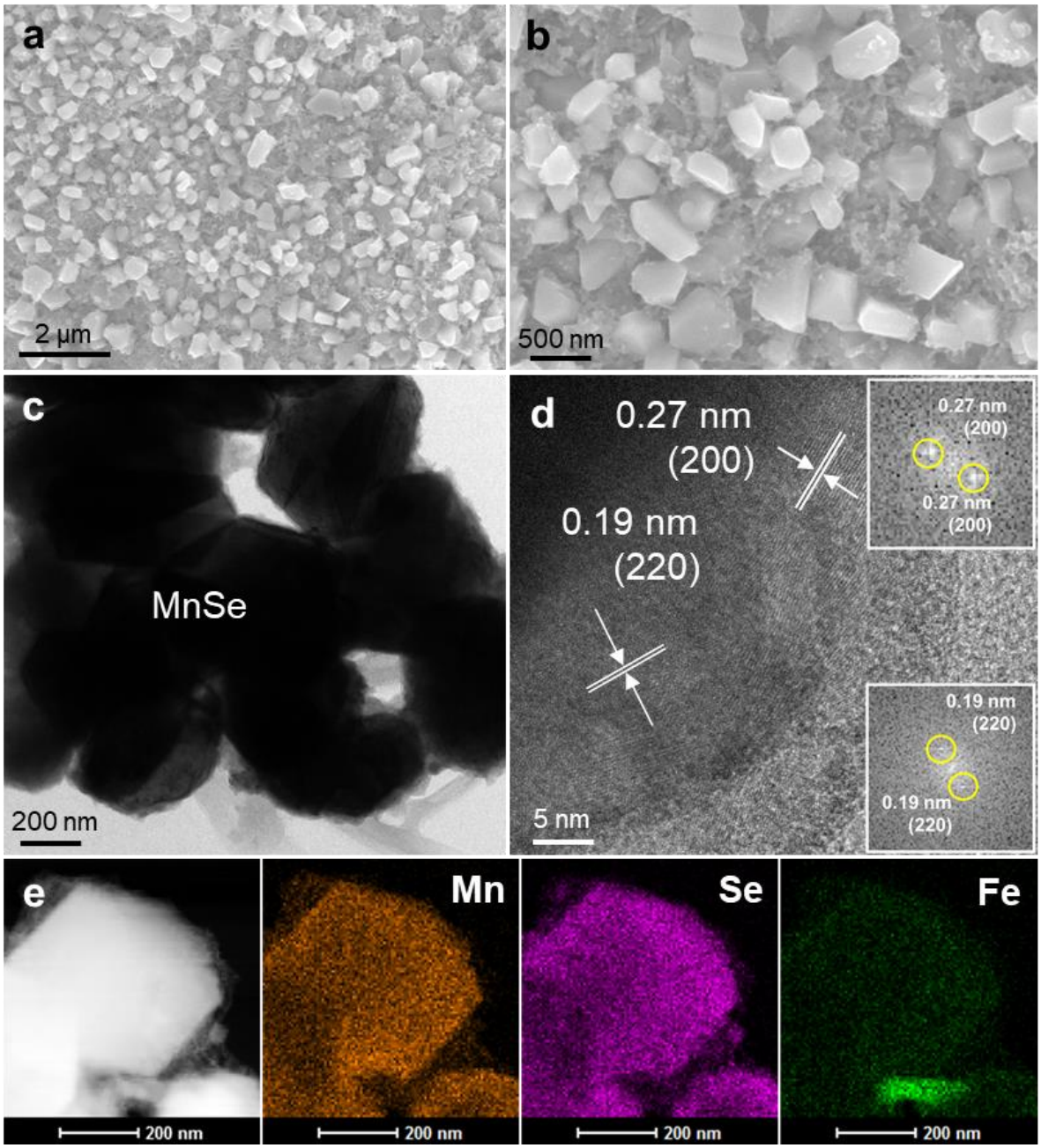

Figure S8. (a,b) SEM images, (c) TEM image, (d) HRTEM image, and (e) TEM-EDS elemental mapping of MnSe/FF. Insets of d show the FFT patterns of corresponding parts.

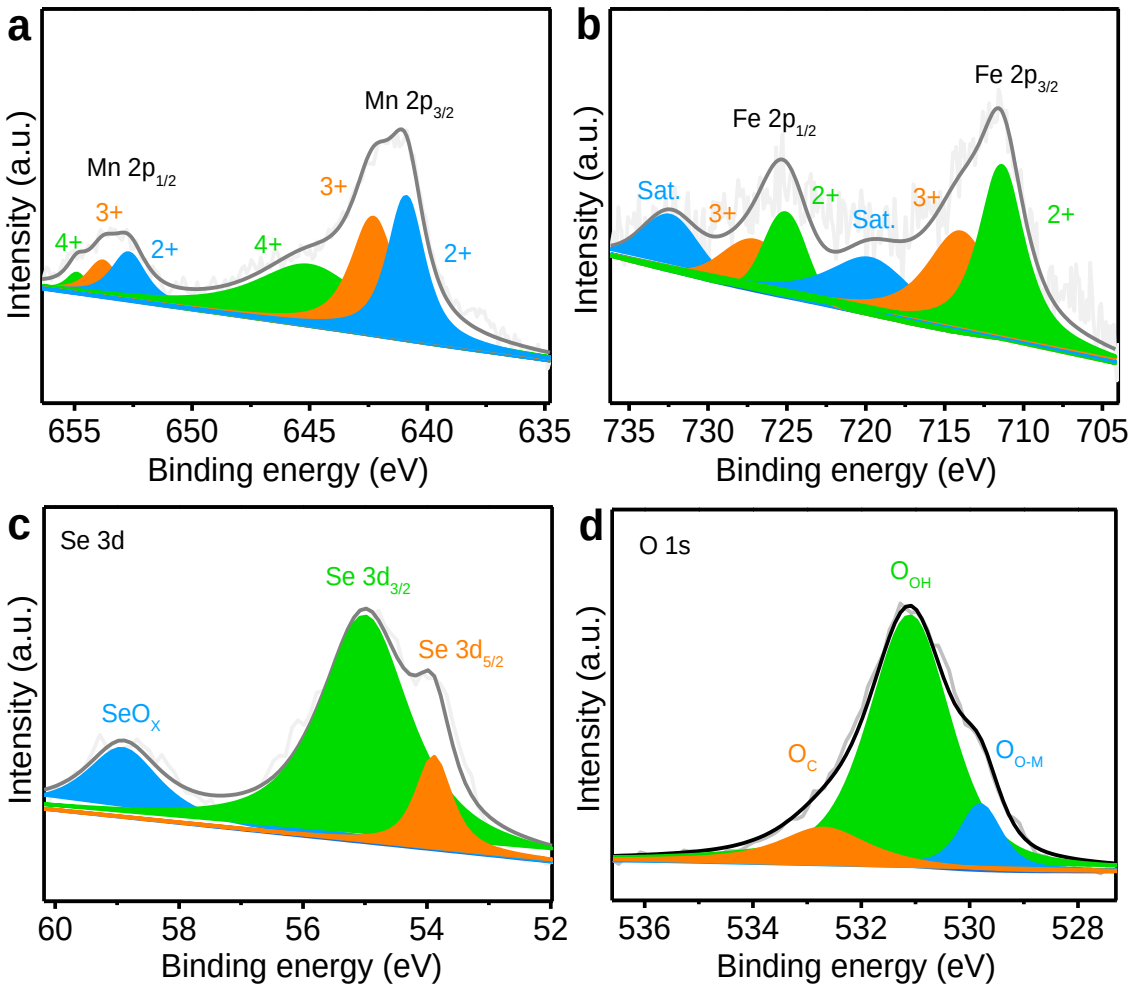

Figure S9. (a-d) XPS Mn 2p (a), Fe 2p (b), Se 3d (c), and O 1s (d) spectra of MnSe/FF.

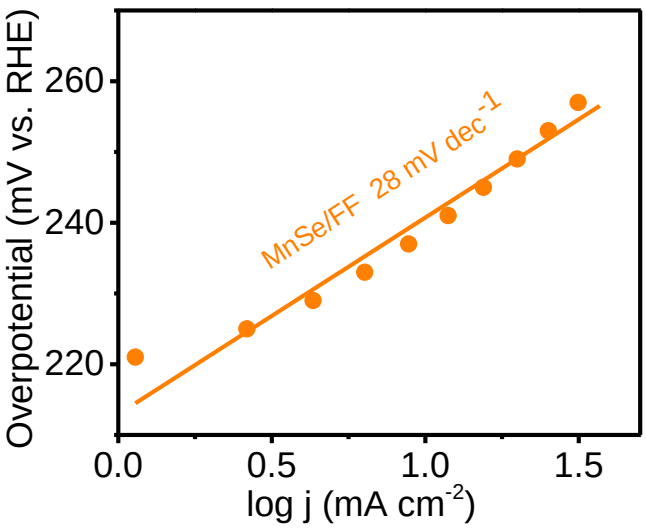

Figure S10. Tafel plot of MnSe/FF.

Table S1. Comparison of the OER performances with reported Mn-based electrocatalysts in 1 M KOH.

Catalyst	Substrate	η_{10} (mV)	Tafel slope (mV dec^{-1})
MnSe in this work	**Ni foam**	**311**	**70**
MnFeSe in this work	**Ni foam**	**247**	**35**
MnSe in this work	**Fe foam**	**239**	**28**
$(Mn_4Co_1)Se_2$ [1]	Powder	274	39
(Co_1Mn_1) Oxide [2]	Powder	221	39.8
Mn doped CoN [3]	Carbon fiber	265	46
$NiMnO_x$ [4]	Ni foam	362	69
the ultrathin δ-MnO_2 [5]	Ni foam	320	40
$Mn_{25}Ru_{75}$ Oxide [6]	Ti plate	259	-
Mn-doped FeOOH [7]	FTO	246	71
MnOOH [7]	FTO	377	131
$Ni_{0.75}Mn_{0.25}$ Oxide [8]	Powder	297	91
(Fe, V, Co, and Ni)-Doped MnO_2 [9]	CFP	390	104.4
MnO_2 [9]	CFP	467	111.7
$Mn_3O_4@Co_xMn_{3-x}O_4$ [10]	Ni foam	284	73.1
Carbon Sheets@$NiMnO_3$ [11]	Powder	250	40
CoMnP [12]	Powder	330	61
$CoMnO_2$ [12]	Powder	390	95
$LiMn_{0.25}Co_{1.75}O_4$ [13]	Powder	430	60
$Fe_{1.1}Mn_{0.9}P$ [14]	Powder	440	39
Mn_3N_2 [15]	Ni foam	270	101
Mn_3N_2 [15]	FTO	390	97
α-MnO_2 [16]	Powder	394	49
b-MnO_2 [17]	Powder	450	78.2
b-MnO_2 [18]	FTO	500	93
Mo doped Mn_2O_3 [19]	FTO	570	75
Mn_3O_4 [20]	SnO_2/ glass	570	-
$MnGa_4$ [21]	Ni foam	291	98

References

[1] X. Zhao, X. Li, Y. Yan, Y. Xing, S. Lu, L. Zhao, S. Zhou, Z. Peng, J. Zeng, *Appl. Catal. B: Environ.* **2018**, *236,* 569-575.

[2] H. Xu, J. Wei, K. Zhang, M. Zhang, C. Liu, J. Guo, Y. Du, *J. Mater. Chem. A* **2018**, *6*, 22697-22704.

[3] Y. Sun, T. Zhang, X. Li, D. Liu, G. Liu, X. Zhang, X. Lyu, W. Cai, Y. Li, *Chem. Commun.* **2017**, *53*, 13237-13240.

[4] Z. Chen, Z. Wang, R. Cai, Y. Xie, J. Yu, X. Long, B. Yang, S. Yang, *Nanoscale* **2020**, *12*, 2472-2478.

[5] Y. Zhao, C. Chang, F. Teng, Y. Zhao, G. Chen, R. Shi, G. I. N. Waterhouse, W. Huang, T. Zhang, *Adv. Energy Mater*. **2017**, *7*, 1700005.

[6] M. P. Browne, H. Nolan, G. S. Duesberg, P. E. Colavita, M. E. G. Lyons, *ACS Catal*. **2016**, *6*, 2408-2415.

[7] M. P. Suryawanshi, U. V. Ghorpade, S. W. Shin, U. P. Suryawanshi, H. J. Shim, S. H. Kang, J. H. Kim, *Small* **2018**, *14*, 1801226.

[8] T. Tian, H. Gao, X. Zhou, L. Zheng, J. Wu, K. Li, Y. Ding, *ACS Energy Lett*. **2018**, *3*, 2150-2158.

[9] Z. Ye, T. Li, G. Ma, Y. Dong, X. Zhou, *Adv. Funct. Mater*. **2017**, *27*, 1704083.

[10] C. Hu, L. Zhang, Z. Huang, W. Zhu, Z.-J. Zhao, J. Gong, *J. Catal.* **2019**, *369*, 105-110.

[11] Z. Wang, J. Li, X. Tian, X. Wang, Y. Yu, K. A. Owusu, L. He, L. Mai, *ACS Appl. Mater. Interfaces* **2016**, *8*, 19386-19392.

[12] D. Li, H. Baydoun, C. N. Verani, S. L. Brock, *J. Am. Chem. Soc.* **2016**, *138*, 4006-4009.

[13] C. W. Cady, G. Gardner, Z. O. Maron, M. Retuerto, Y. B. Go, S. Segan, M. Greenblatt, G. C. Dismukes, *ACS Catal*. **2015**, *5*, 3403-3410.

[14] D. Li, H. Baydoun, B. Kulikowski, S. L. Brock, *Chem. Mater.* **2017**, *29*, 3048-3054.

[15] C. Walter, P. W. Menezes, S. Orthmann, J. Schuch, P. Connor, B. Kaiser, M. Lerch, M. Driess, *Angew. Chem. Int. Ed.* **2018**, *57*, 698-702.

[16] G. Yan, Y. Lian, Y. Gu, C. Yang, H. Sun, Q. Mu, Q. Li, W. Zhu, X. Zheng, M. Chen, J. Zhu, Z. Deng, Y. Peng, *ACS Catal*. **2018**, *8*, 10137-10147.

[17] J. Kim, J. S. Kim, H. Baik, K. Kang, K. Lee, *RSC Adv*. **2016**, *6*, 26535-26539.

[18] M. Fekete, R. K. Hocking, S. L. Y. Chang, C. Italiano, A. F. Patti, F. Arena, L. Spiccia, *Energy Environ. Sci*. **2013**, *6*, 2222.

[19] S. E. Balaghi, C. A. Triana, G. R. Patzke, *ACS Catal*. **2020**, *10*, 2074-2087.

[20] A. Ramírez, P. Hillebrand, D. Stellmach, M. M. May, P. Bogdanoff, S. Fiechter, *J. Phys. Chem. C* **2014**, *118*, 14073-14081.

[21] P. W. Menezes, C. Walter, J. N. Hausmann, R. Beltran-Suito, C. Schlesiger, S. Praetz, V. T. Verchenko, A. V. Shevelkov, M. Driess, *Angew. Chem. Int. Ed.* **2019**, *58*, 16569-16574.

Table S2. Comparison of the OER performances of MnFeSe with recently reported Se-based electrocatalysts in 1 M KOH.

Catalyst	Substrate	η_{10} (mV)	η_{20} (mV)	Tafel slope (mV dec^{-1})
MnSe in this work	**Ni foam**	**311**	**331**	**70**
Fe-MnSe in this work	**Ni foam**	**247**	**259**	**35**
MnSe in this work	**Fe foam**	**239**		**28**
NiSe [1]	Ni foam		270	64
$NiSe_2$ [2]	Powder	287		87.2
$Ni_xFe_{1-x}Se_2$ [3]	Ni foam	195		28
$(Ni,Co)Se_2$ [4]	Graphene aerogel	250		70
CoSe [5]	Ti mesh	292		69
$CoSe_2$ [6]	Powder	330		79
$CoSe/MoSe_2$ [7]	Powder	262		54.9
$FeSe_2$ [8]	Ni foam	245		-
$FeSe_2$ [9]	Ni foam	330		48.1
$(Co_{0.21}Ni_{0.25}Cu_{0.54})_3Se_2$ [10]	Au-coated glass	272		53.3
Co0.85Se [11]	Powder	290		81
Li-$IrSe_2$ [12]	Powder	270		-

References

[1] C., N. Tang, Cheng, Z. Pu, W. Xing, X. Sun, *Angew. Chem. Int. Ed.* **2015**, *54,* 9351-9355.

[2] H. Li, S. Chen, H. Lin, X. Xu, H. Yang, L. Song, X. Wang, *Small* **2017**, *13,* 1701487.

[3] X. Xu, F. Song, X. Hu, *Nat. Commun.* **2016**, *7*, 12324.

[4] X. Xu, H. Liang, F. Ming, Z. Qi, Y. Xie, Z. Wang, *ACS Catal*. **2017**, *7*, 6394-6399.

[5] T. Liu, Q. Liu, A. M. Asiri, Y. Luo, X. Sun, *Chem. Commun.* **2015**, *51*, 16683-16686.

[6] X. Liu, Y. Liu, L.-Z. Fan, *J. Mater. Chem. A* **2017**, *5*, 15310.

[7] M. Yuan, S. Dipazir, M. Wang, Y. Sun, D. Gao, Y. Bai, M. Zhang, P. Lu, H. He, X. Zhu, S. Li, Z. Liu, Z. Luo, G. Zhang, *J. Mater. Chem. A* **2019**, *7*, 3317-3326.

[8] C. Panda, P. W. Menezes, C. Walter, S. Yao, M. E. Miehlich, V. Gutkin, K. Meyer, M. Driess, *Angew. Chem. Int. Ed.* **2017***, 56,* 10506-10510.

[9] R. Gao, H. Zhang, D. Yan, *Nano Energy* **2017**, *31*, 90-95.

[10] X. Cao, E. Johnson, M. Nath, *J. Mater. Chem. A* **2019**, *7*, 9877-9889.

[11] J. Yu, G. Cheng, W. Luo, *Nano Res.* **2018**, *11*, 2149-2158.

[12] T. Zheng, C. Shang, Z. He, X. Wang, C. Cao, H. Li, R. Si, B. Pan, S. Zhou, J. Zeng, *Angew. Chem. Int. Ed.* **2019**, *58,* 14764-14769.

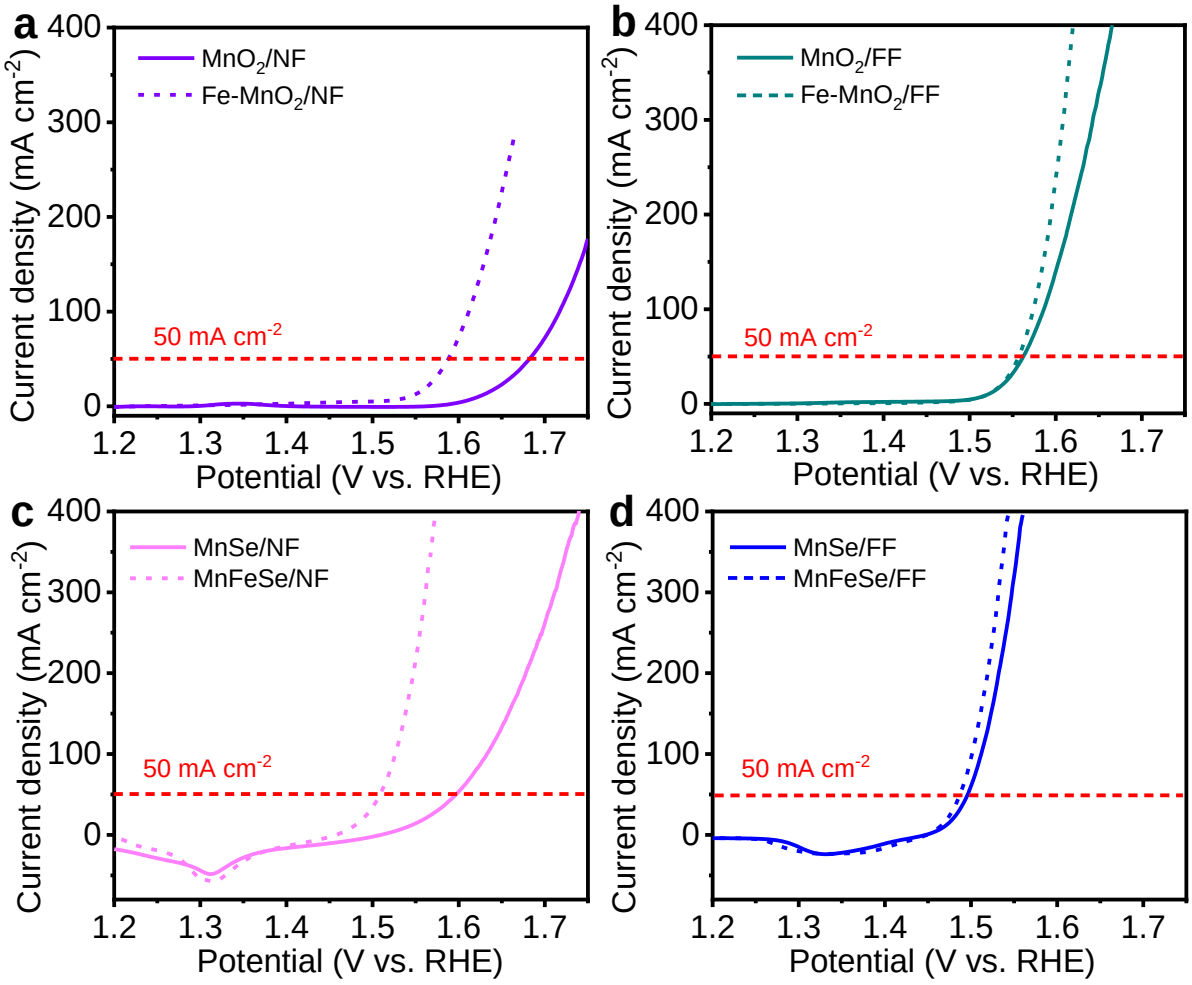

Figure S11. (a) LSV curves of MnO_2/NF and Fe-MnO_2/NF; (b) LSV curves of MnO_2/FF and Fe-MnO_2/FF; (d) LSV curves of MnSe/NF and MnFeSe/NF; (d) LSV curves of MnSe/FF and MnFeSe/FF. All tests were measured in 1 M KOH.

For comparison, Fe-MnO_2/FF was prepared as MnO_2/FF was immersed into 10 mM $Fe(NO_3)_3$ aqueous solution for cation exchange. The, the Fe-MnO_2/FF was treated in the same approach with MnSe/NF (see experimental) to form MnFeSe/FF.

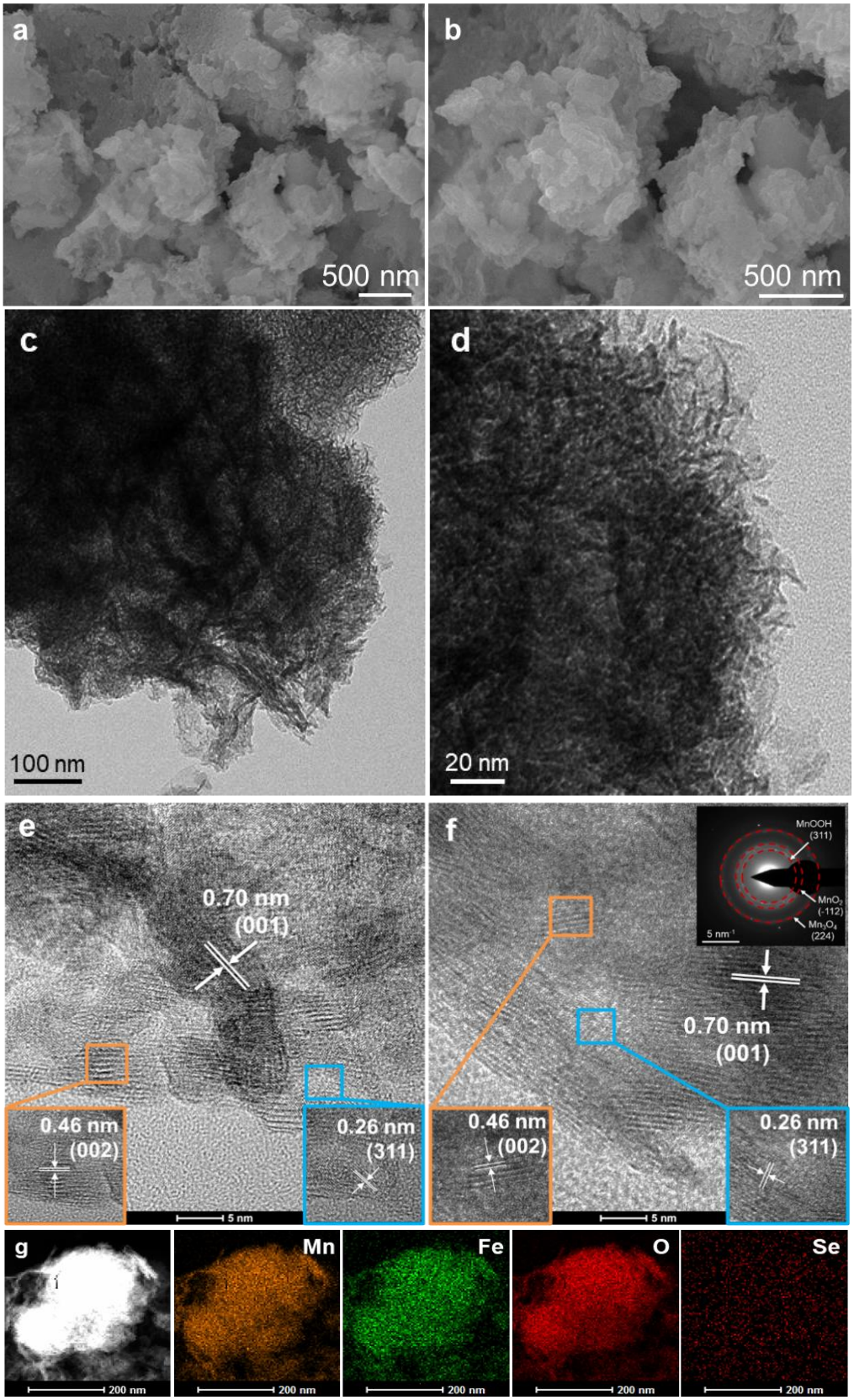

Figure S12. (a,b) SEM images, (c,d) TEM images, (e,f) HRTEM images, (g) TEM-EDS elemental mapping of MnFeSe/NF after chronopotentiometric measurement of 20 h. Insets of e show the FFT patterns; insets of f show the FFT patterns and SAED pattern.

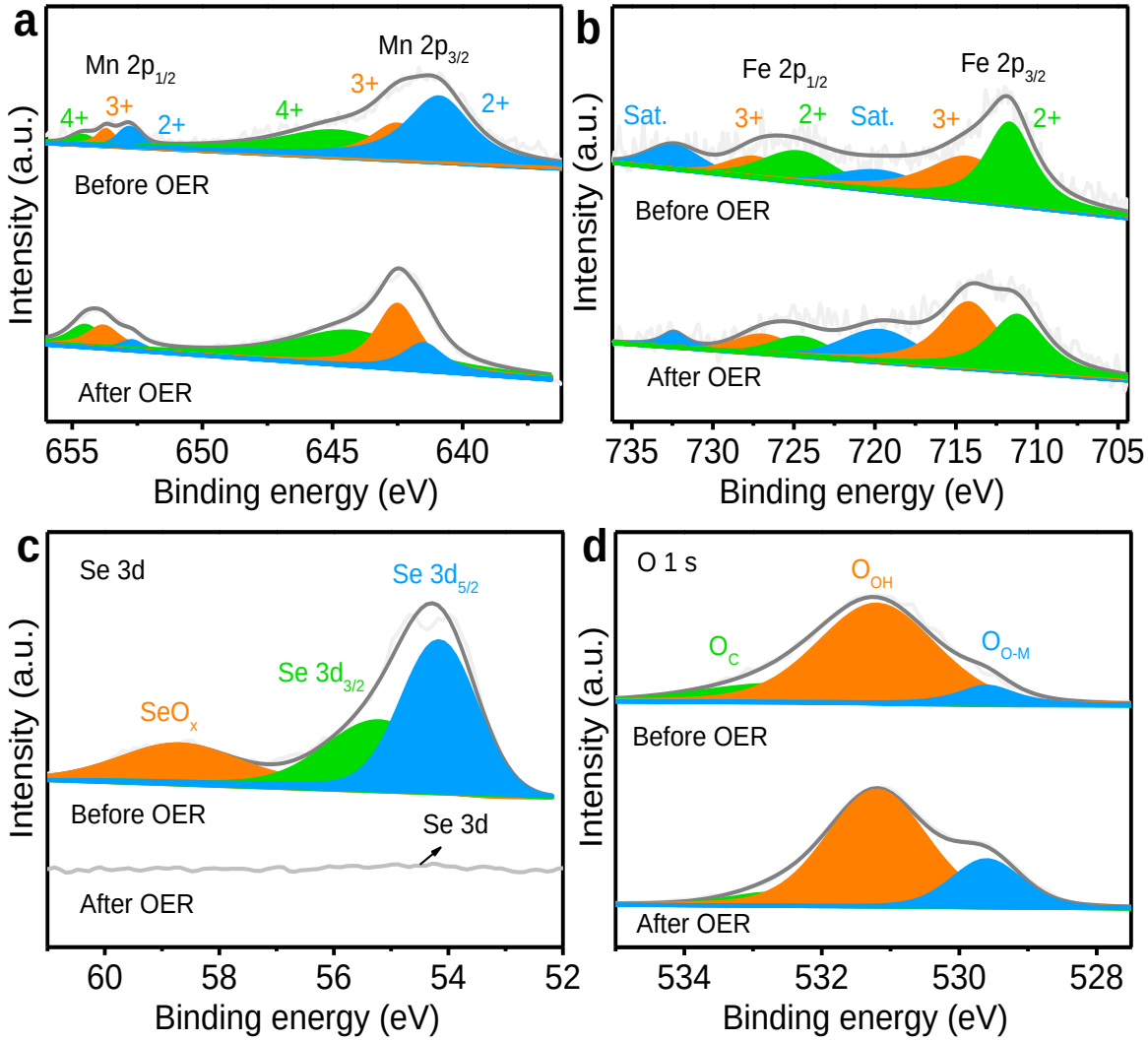

Figure S13. (a-d) XPS Mn 2p (a), Fe 2p (b), Se 3d (c), and O 1s (d) spectra of MnFeSe/NF before and after chronopotentiometric measurement.

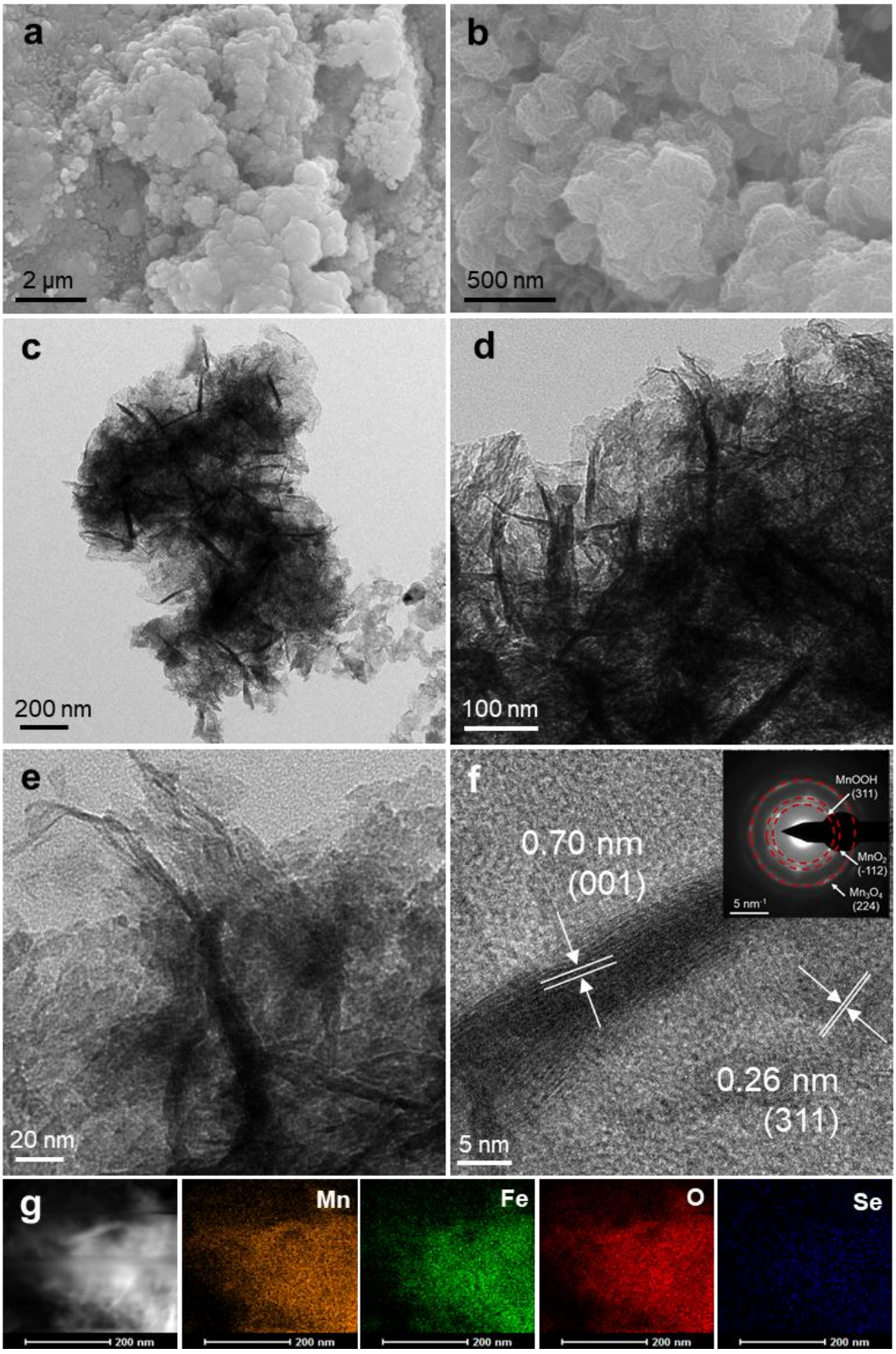

Figure S14. (a,b) SEM images, (c-e) TEM images, (f) HRTEM image, and (g) TEM-EDS elemental mapping of MnSe/FF after chronopotentiometric measurement of 20 h. Inset of f shows the SAED pattern.

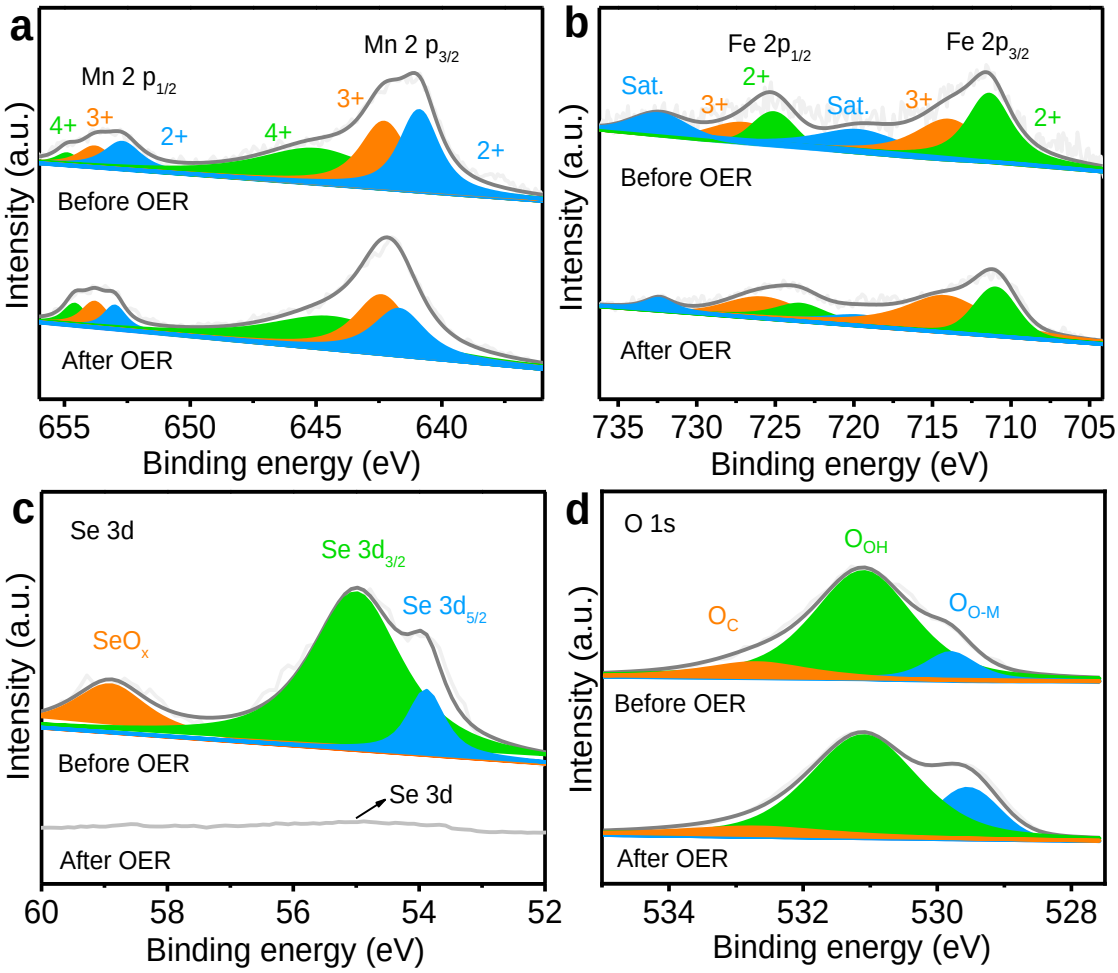

Figure S15. (a-d) XPS Mn 2p (a), Fe 2p (b), Se 3d (c), and O 1s (d) spectra of MnSe/FF before and after chronopotentiometric measurement.

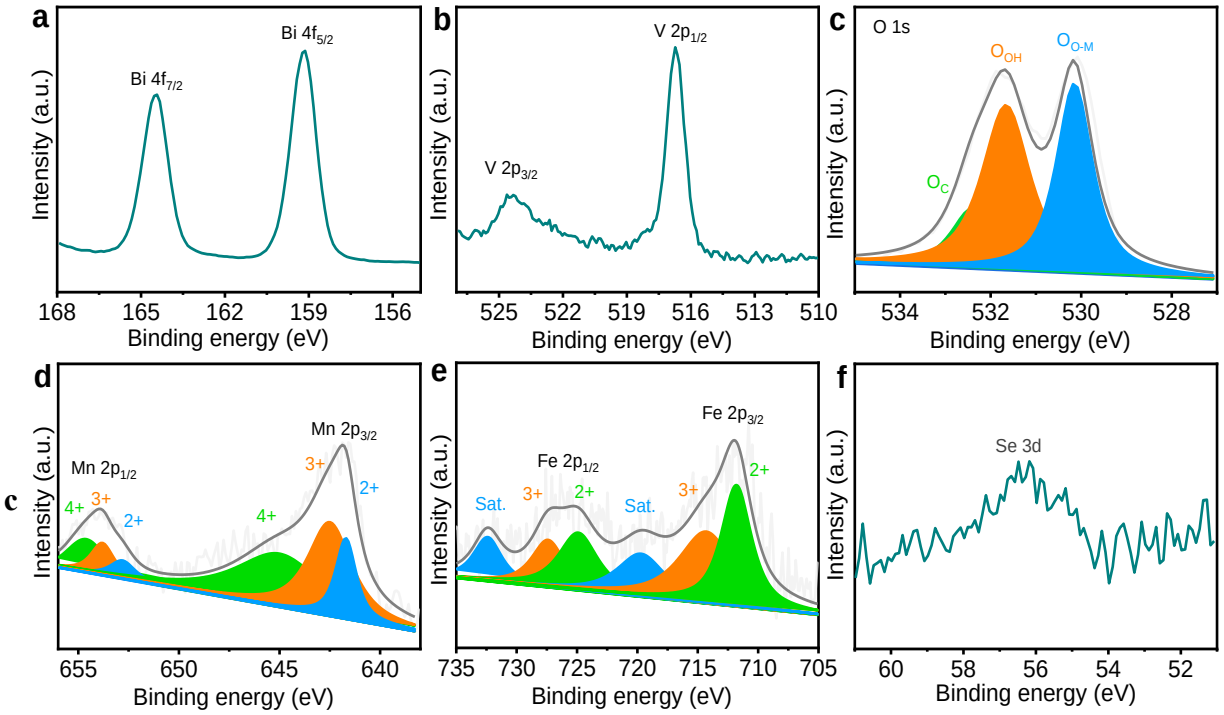

Figure S16. (a-f) XPS Bi 4f (a), V 2p (b), O 1s (c), Mn 2p (d), Fe 2p (e), and Se 3d (f) spectra of Se,Fe-MnO_x/BVO.

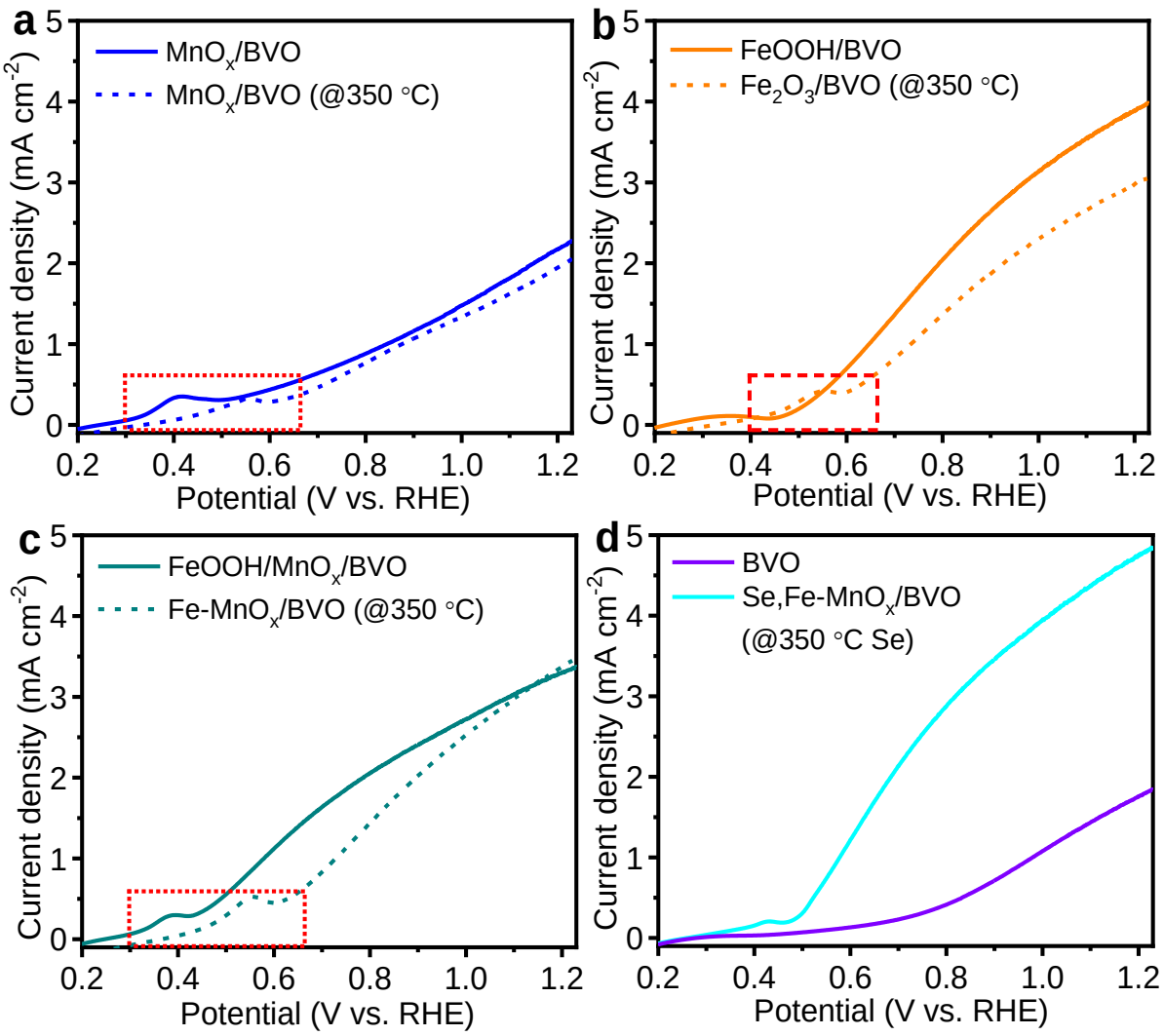

Figure S17. (a) LSV curves of MnO_x/BVO without and with annealing treatment; (b) LSV curves of FeOOH/BVO and Fe_2O_3/BVO without and with annealing treatment; (c) LSV curves of FeOOH/MnO_x/BVO without and with annealing treatment. The annealing condition of (a),(b), and (c) was at 350 °C without Se powder; (d) LSV curves of BVO and Se,Fe-MnO_x/BVO. The Se,Fe-MnO_x/BVO was annealed at 350 °C with Se powder. The PEC performances were performed in 1 M KBi under AM 1.5G (100 mA cm^{-2}) illumination.

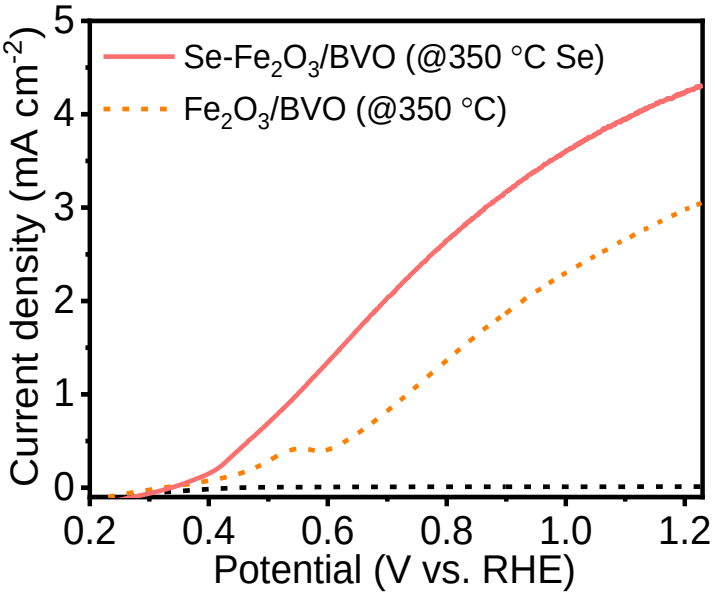

Figure S18. LSV curves of Fe_2O_3/BVO and Se-Fe_2O_3/BVO in 1 M KBi under AM 1.5G (100 mA cm^{-2}) illumination. Fe_2O_3/BVO and Se-Fe_2O_3/BVO samples were annealed at 350 °C without and with Se power, respectively.

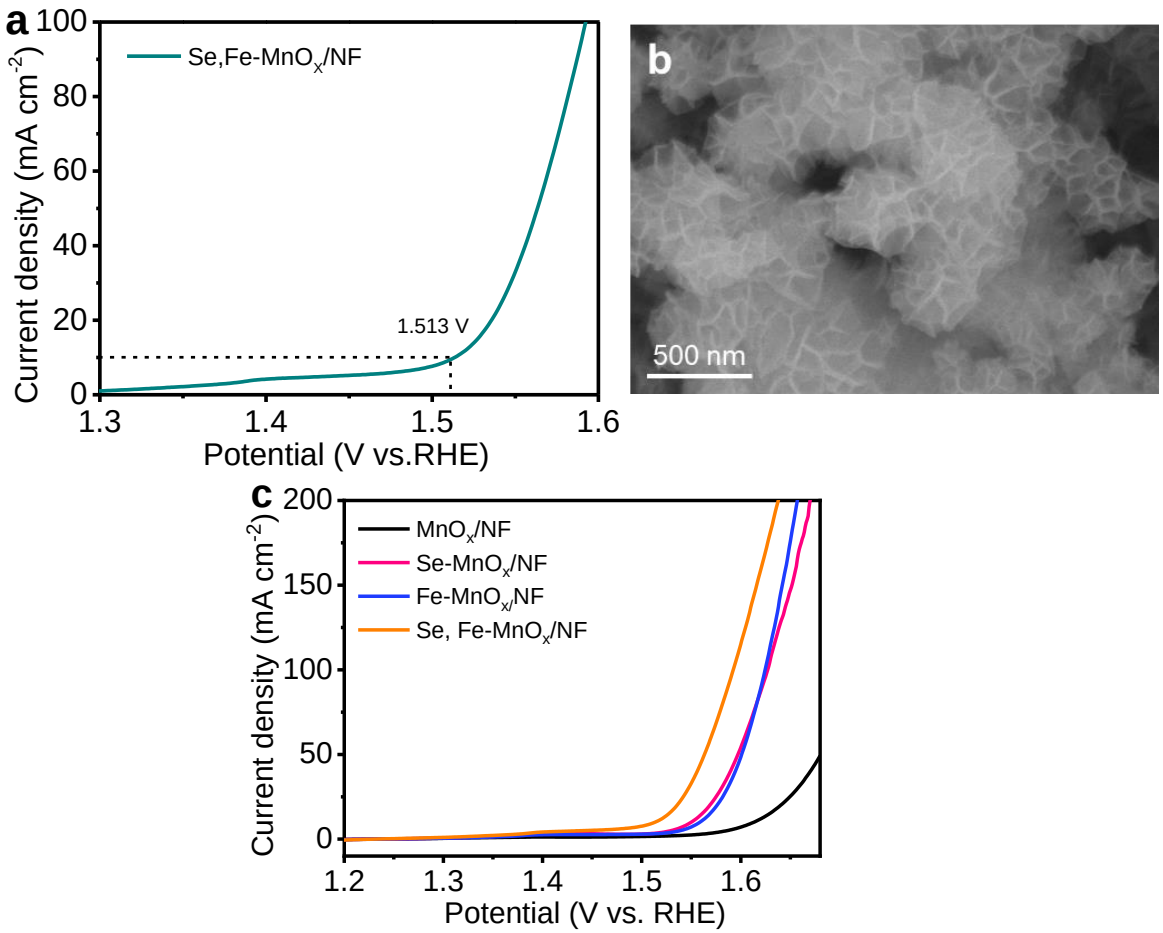

Figure S19. (a) LSV curve of Se,Fe-MnO_x/NF in 1 M KOH; (b) SEM image of corresponding sample. The selenization was annealed at 350 °C with Se powder, replacing the hydrothermal condition; (c) comparison of LSV curves of MnO_x/NF, Se-MnO_x/NF, Fe-MnO_x/NF, and Se,Fe-MnO_x/NF in 1 M KOH.

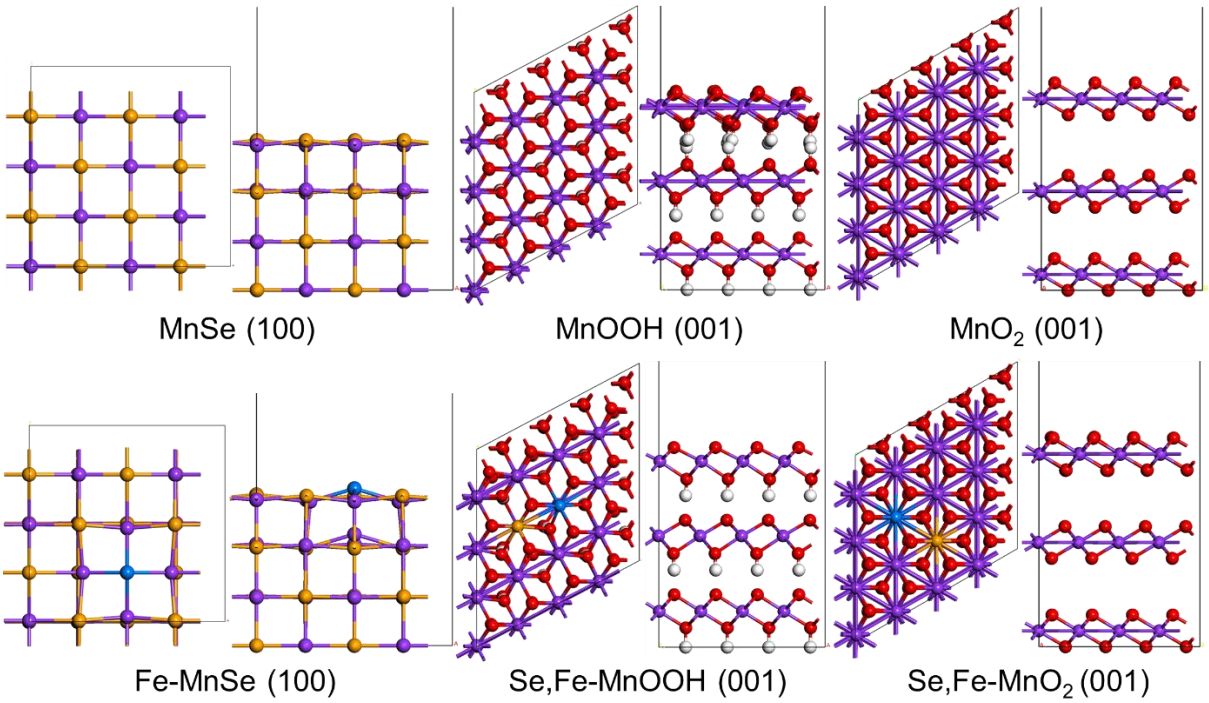

Figure S20. The top and side view structures of MnSe (100), Fe-MnSe (100), MnOOH (001), Se,Fe-MnOOH (001), MnO_2 (001), and Se,Fe-MnO_2 (001) surfaces. The Mn, Fe, Se, O and H atoms are in purple, blue, orange, red, and white, respectively.

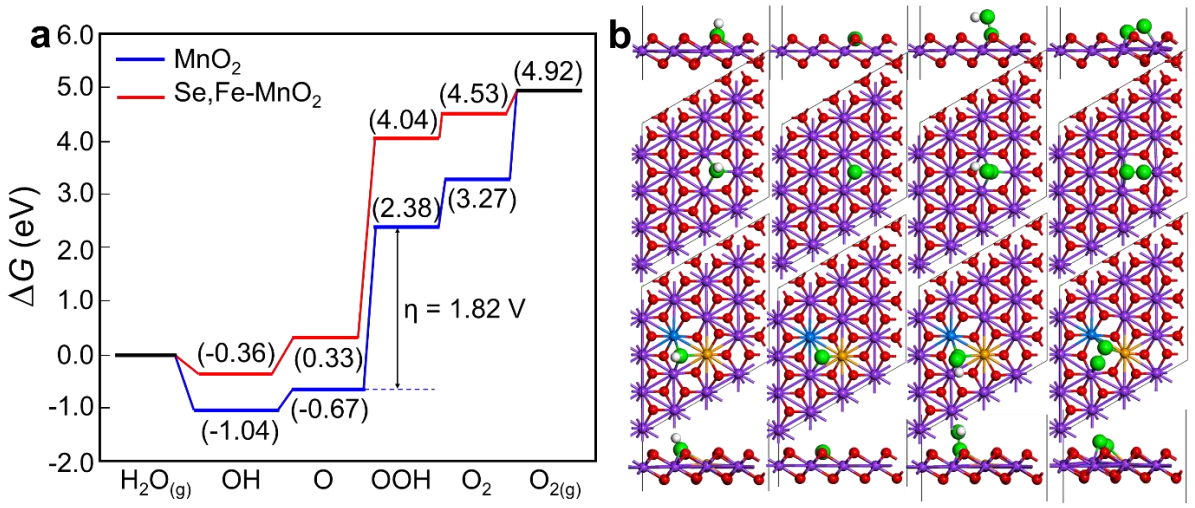

Figure S21. (a) The calculated free-energy profiles of the OER on MnO_2 and Se,Fe-MnO_2 catalysts under 0 V; (b) as well as the top and side view structures of OH, O, and OOH adsorptions on the two models; the Mn, Fe, Se, O, and H atoms are in purple, blue, orange, red, and white, respectively; to make the distinction, the O atom from H_2O is given in green.

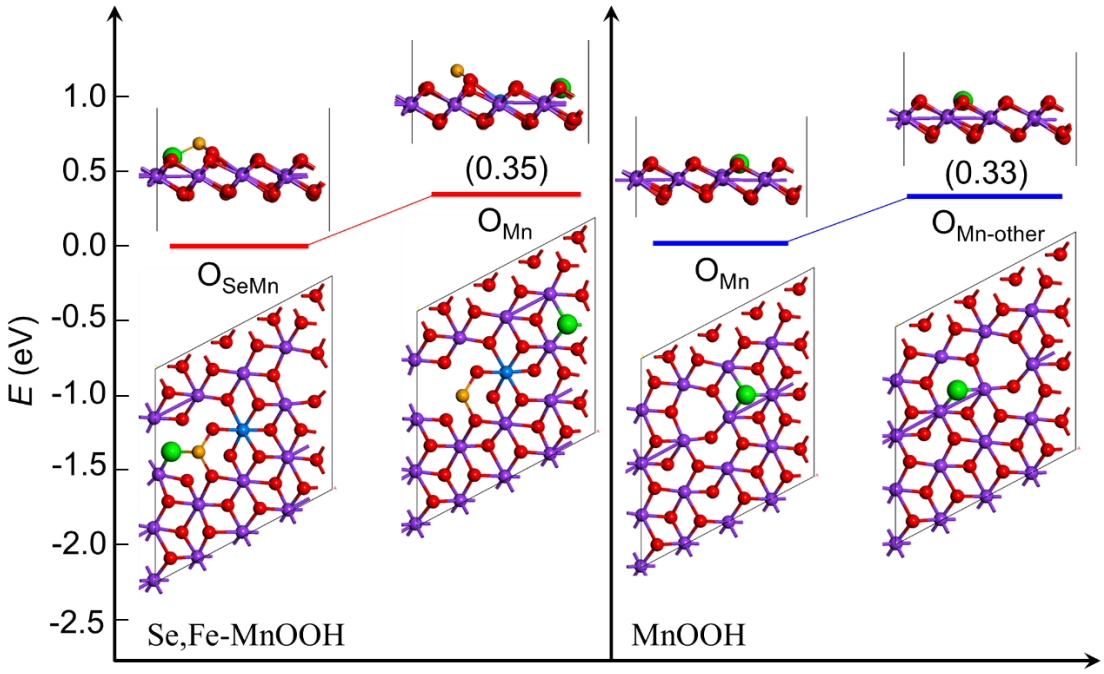

Figure S22. The energy profiles for the atomic O migration on Se,Fe-MnOOH and MnOOH surfaces; the Mn, Fe, Se, and O atoms are in purple, blue, orange, and red, respectively; to make the distinction, the O atom from H_2O is given in green.

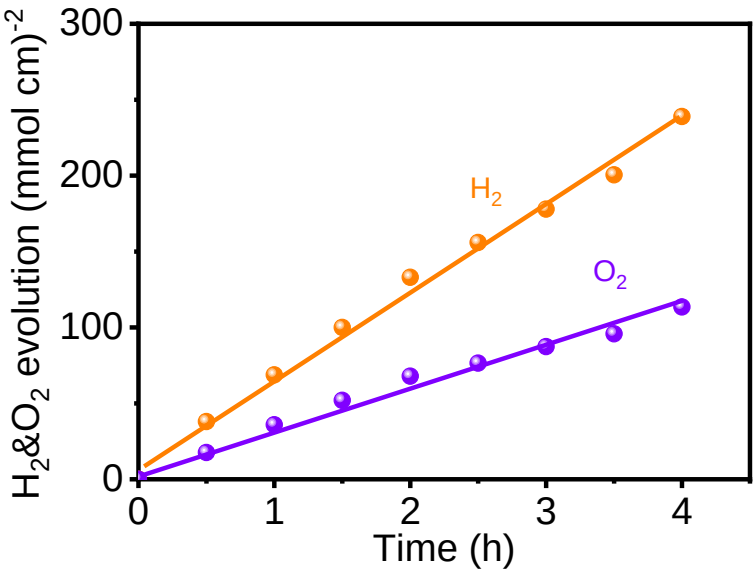

Figure S23. Gas evolutions detected by gas chromatography of MnFeSe/NF at 10 mA cm^{-2} for 4 h in 1 M KOH.